



Developing flood vulnerability curve for rice crop using remote sensing and hydrodynamic modeling



Vempi Satriya Adi Hendrawan^{a,*}, Daisuke Komori^{a,b}

^a Graduate School of Environmental Studies, Tohoku University, Sendai 980-8579, Japan

^b Graduate School of Engineering, Tohoku University, Sendai 980-8579, Japan

ARTICLE INFO

Keywords:

Crop yield loss
Flood
Remote sensing
Submergence
Vulnerability curve

ABSTRACT

The use of flood damage functions, or vulnerability curves, as a relationship between the intensity of the process (hazard) and the degree of potential loss of the exposed elements plays an important role in flood risk assessment. In terms of disaster risk reduction, a vulnerability curve is a helpful tool to quickly evaluate loss and conduct immediate decision making. This study proposes flood vulnerability curves for rice crop using crop yield loss estimated by crop statistics and remote-sensing modeling as a loss indicator. Flood parameters (depth, velocity, and duration) were simulated using a hydrodynamic model. Thus, the degree of crop yield loss and flood characteristics could be compared to derive vulnerability curves. In this study, we used a case study of the 2007 flood in the Solo river basin of Indonesia. Our results show that the relationship between the intensity of flood parameters and the degree of rice crop yield loss fits logarithmic regression functions, where water depth is considered the most significant parameter in loss estimation. Moreover, the minimum values of water depth, flow velocity, and duration relationship, that induce loss are 0.2 m, 0.03 m/s, and 8 days, respectively, while the maximum values, that induce complete yield loss, are 5.2 m, 0.08 m/s, and 22 days. This study's framework can be potentially used to obtain flood vulnerability curve or flood damage function, particularly for data-scarce regions.

1. Introduction

As meteorological disasters, floods have influenced the agriculture sector severely in recent years [1]. In Asian countries, most lowland rice-cultivation areas are prone to flooding [2]. Rice-producing countries located in Monsoon Asia account for ~90% of the world's both harvested area and production of rice [3]. They are characterized by abundant precipitations, multiple growing seasons, and warmer temperatures, which bring benefits to crop growth and yield. Although the nature of the paddy rice crop can be well adapted extensively in an inundated lowland environment, rice crop has been affected often by the adverse impact of extreme rainfall during primary growing season [4,5]. These rice cultivation areas can be partially or completely submerged at different stages of crop growth and experience fast or stagnant floods. These conditions often affect crops and induce damages [2,6,7].

There are only a few studies specifically focusing on crop impact due to flood [8,9]. Compared to other sectors, such as the residential, industry, and infrastructure sectors, evaluation of agricultural flood losses or damage is often neglected, or only roughly estimated. For instance,

for the same hazard and exposure, the urban sector often experiences much larger losses than the agriculture [10,11]. However, as pointed out by Klaus et al. [12], the agricultural losses due to flood can be higher in the case of frequent floods, where there is no flood prevention infrastructure, such as in rural areas [11]. Agricultural losses due to flood become a major concern in such regions, especially where large populations mainly rely on agricultural activities [13]. In addition, the flood impact can even increase since an emerging concept was proposed to allow agricultural land to be flooded and thus to protect more vulnerable areas, which are generally urban areas [14]. Deeper understanding is required, as the importance of comprehensive flood damage assessment in agriculture is increasing [12].

To understand flood impact characteristics on agricultural losses, a common method using a damage function has been widely used [15–17]. This damage function is known in risk assessment as a vulnerability curve [18]. Vulnerability curve in this context expresses physical vulnerability as a relationship between the intensity of the process (hazard) and the degree of potential loss of the exposed elements (e.g., a certain crop type) [19,20]. Flood risk is defined as a function of

* Corresponding author.

E-mail addresses: vempi@dc.tohoku.ac.jp, vempisatriya@gmail.com (V.S.A. Hendrawan), daisuke.komori.e8@tohoku.ac.jp (D. Komori).

hazard (e.g., flood depth), exposure (e.g., assets exposed), and vulnerability component (susceptibility of the exposed element to the hazard) [20,21]. Thus, the vulnerability curves, which represent the vulnerability component, play an important role in flood risk assessment and have large contributions to the overall risk [22]. In terms of disaster risk reduction, a vulnerability curve is a helpful tool for rapid assessment of loss and immediate decision making, as it uses a proxy of hazard obtained by modeling to estimate losses. Timely and better estimates of flood impact characteristics on the agricultural losses can support agricultural policy, insurance appraisal, and various decision processes [9–11,23,24].

To derive the damage function (vulnerability curve), at least two standard approaches have been used: experimentation and ex-post damage data [17,24]. The first approach has been used to observe the biophysical response of plants to specific conditions of flood submergence. However, as pointed out by Brémond et al. [24], experimentation requires a lot of effort and does not correspond to methods applied in other sectors to assess damages. For instance, experimental work done by Ganji et al. [25] aimed to develop a rice crop loss and flood hydraulic parameters relationship by a set of laboratory tests. However, a clear relationship between the crop yield loss and common flood parameters (depth and velocity) could not be obtained, revealing instead the Reynolds number as the best parameter to estimate rice crop loss. The second approach used ex-post damage data to derive an empirical relationship between flood depth and/or duration (sometimes including crop season) and the associated crop yield loss. There are several existing damage databases and models, including HOWAS in Germany [26], USACE in the United States [27], Multi-Coloured Manual in the United Kingdom [28], and flood damage statistics in Japan [29]. Most of them are limited only to urban damage [10]. Moreover, due to the limitations of historical damage databases, data collection based on experts or interview-based knowledge can also be conducted, such as in Brémond and Grelot [30]. In the case of rice crops, studies have been widely conducted in the Southeast Asian river basin to obtain flood vulnerability curves for rice crop from empirical data and farmer interviews [31,32].

Despite its popularity, the use of the flood vulnerability curve in crop damage assessment is limited in regions where vulnerability curves or standard methodologies have been established. Moreover, in data-scarce regions flood damage assessments of the crops often use other existing vulnerability curves or models, developed elsewhere [33,34]. However, as Pivot and Martin [35] pointed out, vulnerability curves are very context-specific, and physical conditions may vary from one situation to another. Therefore, the use of other vulnerability curves without justification may lead to inaccurate results [16].

Particularly in the case of rice crop, there were numerous studies of plant physiology that have investigated the crop response to waterlogging or submergence [36,37]. An understanding of rice crop's tolerance mechanism to the floods has been developed based on experiments, using some control conditions including rice variety, submergence duration, depth, and crop growth stage. However, little has been explicitly used for wide-scale flood assessments application (e.g., river basin or country scale), as conditions may not be the same for laboratory and field-scale observation. In addition, despite the clear coping mechanism to flooding, there are wide variations in existing flood vulnerability curves for rice crop (e.g., in Japan [29,38,39], Mekong Delta [40], and Philippines [31]). This relationship is highly attributed to rice variety, physical condition of a specific area, and other factors. Therefore, the challenge of understanding rice crop behavior against flooding emerges when the threshold between "loss" and "no loss" vary even for the same crop.

Given the gaps mentioned above, this study aims to develop a flood vulnerability curve or damage function for rice crop as a relationship between the degree of crop yield loss and the intensity of flood parameters, using a modeling approach. In addition, we expected to obtain a damageable flood, which has a specific intensity that may induce yield

loss. The expected findings would enrich the current understanding of the impact of flood submergence on rice crops. Moreover, this study provides an operational approach for a specific case study of an extreme flood event, with limited flood damage data and a lack of understanding of the flood vulnerability curve for rice crops.

To achieve this purpose, we set several objectives, as follows: 1) obtain the vulnerability curve as a relationship between the degree of yield loss and the intensity of flood parameters, 2) investigate the most significant flood parameter affecting crop yield loss, and 3) discuss damageable flood intensity on rice crop yield based on the flood parameter obtained in the previous step.

2. Case study

The study area consists of rice paddy fields located in Bengawan Solo river basin (hereafter Solo river basin), the largest river basin in Java Island, Indonesia, with a total catchment of about 16,000 km². It runs 600 km along the Central and East Java Provinces and flows northeast into the coast of Java Sea, northwest of Surabaya city (Fig. 1). In 1981, the Wonogiri multipurpose dam, with a capacity of 730×10^6 m³, was built for flood control and water storing for agricultural purposes [41].

The basin is one of the most important agricultural areas in the country, the rice field area being ~50% of the total rice field area of East Java [42]. It yields a significant amount of rice production in Java and even on the national scale. The agriculture sector contributes significantly to the country's food security and economic growth, as it accounts for approximately 14% of the country's total GDP [43]. Therefore, damage to agriculture is a significant issue for the country, since the agriculture sector plays an essential role in its economy.

The basin has a humid tropical monsoon climate with southeast and northwest monsoons. The southeast monsoon usually starts in May and extends to October, influenced by Australian continental air masses (dry season); the northwest monsoon occurs from November to March, bringing moist air from Asia and the Pacific Ocean (rainy season). In addition, tropical cyclones and large-scale storms also often influence the climate in this region. The annual average rainfall is ~2100 mm; according to the Solo river basin management organization [44], the amount of rainfall within the rainy season, alone, accounts for ~80% of the total annual rainfall.

The basin's valley area is characterized by low land zones, mostly used for rice crop cultivation (Fig. 1). The river has a gentle slope bed, meandering channel, and generally low riverbank, passing through wide lowland paddy fields frequently flooded during the rainy season. The rainy season in this basin overlaps with the primary rice crop growing season, which is often disturbed by flooding that causes significant crop yield loss and damage.

Rice is the main cultivar in the area, and 63% of the basin's agricultural area is occupied by rice fields. Usually, farmers start to cultivate the first rainy season rice during the onset of the rainy season. The second period of rainy season cultivation occurs from around March to June [45]. During dry season, dry crops (e.g., maize, beans, cassava, sweet potato) are planted between May and September (Fig. 2). In some parts of the region, especially where irrigation is regularly provided, rice is cultivated in the dry season as the third rice cropping season (usually from July to October).

From late December 2007 until early January 2008, an extreme rainfall occurred in the upstream of the Solo river basin; it induced an extreme flood in the Solo river, affecting people, and producing damage in some sectors. Precipitations reached 137 mm/day (areal average), which was equivalent to a ~100-year return period of rainfall intensity in the upstream part of the river basin [46]. According to the Dartmouth Flood Observatory [47], approximately 60,000 people were displaced due to this flood and 127 people died. The agricultural damage reached 60,630 ha of paddy fields [48]. It was reported that the greatest losses were caused by flooding that occurred just before the harvest time [45]. In this study, we modeled the 2007 flood events in the Solo river basin,

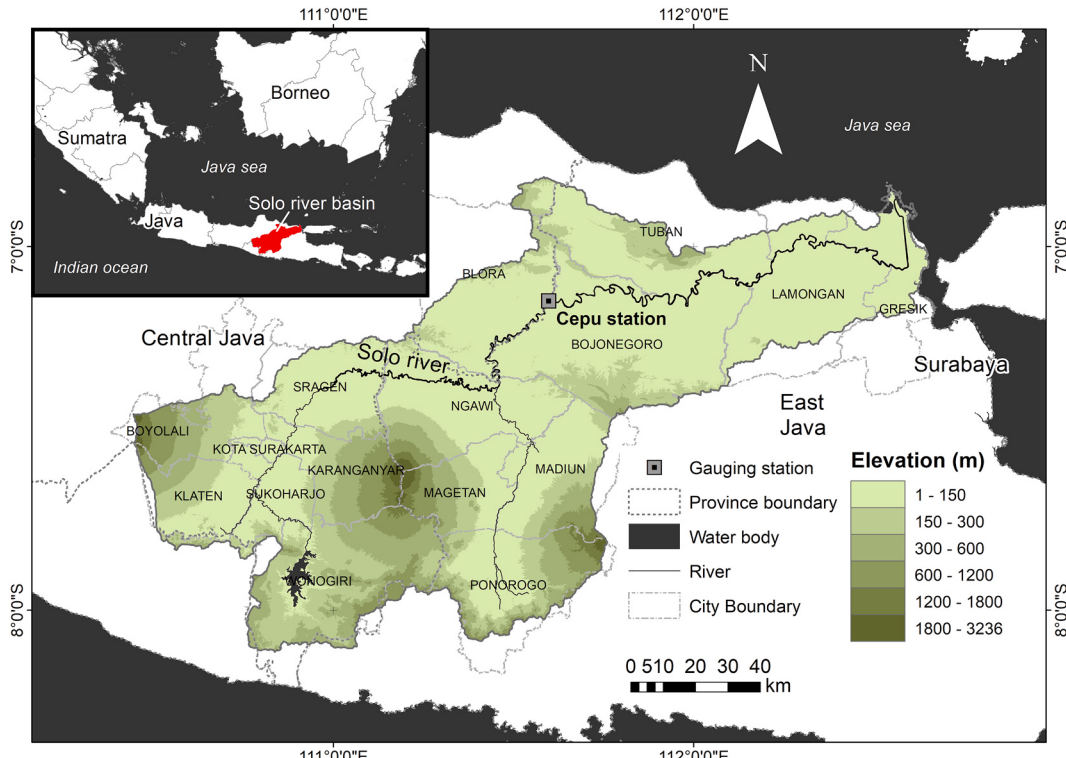


Fig. 1. Solo river basin map and administrative cities.

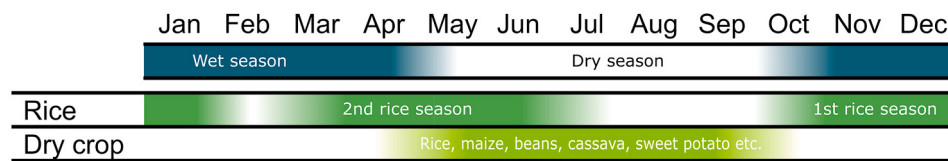


Fig. 2. Cropping calendar of the study area.

since it was considered the biggest flood since 1994 and caused substantial agricultural losses. We reconstructed the flood event in the river basin for a period extending from December 23, 2007 to January 17, 2008.

3. Materials and methods

Remote sensing data have gained much attention due to their advantage of covering wide areas, high temporal resolution, relatively lower cost, and availability of a variety of data [23,49,50]. The use of remote sensing allows identification of the spatiotemporal characteristics of vegetation conditions using Vegetation Indices (VIs). Here, we adopted the framework proposed by Chen et al. [51], which integrated a remote sensing-based crop yield loss model and a flood simulation model to understand the relationship between flood characteristics and the degree of crop losses. Crop yield loss was estimated by multiple linear regression between annual crop yield statistics as dependent variables, and monthly Normalized Difference Vegetation Index (NDVI) and Enhanced Vegetation Index (EVI) during the crop growth season as predictors. Crop pattern and yield loss model were based on HJ-1A/B CCD imagery. The two-dimensional hydraulic model coupled with a hydrologic model was used to simulate a flood event. The comparison between spatial crop yield losses and flood dynamics was then used to understand the flood characteristics-crop losses relationship. Chen's study focused on spring corn, soybean, and rice as target crops and applied the framework for a flood event that occurred in the Jilin

province, Northeast China, in August 2013.

This study further investigates the applicability of the framework in a case study with different climate and geographical conditions for monsoon rice crop in a multiple cropping environment. Furthermore, this study demonstrates more potential approaches as an improvement of the previous study [51]. The proposed refinements conducted in this study are as follows:

1. Pre-processing of the remote sensing data such as cloud pixel removal and time series smoothing. This is necessary, especially when dealing with optical remote sensing data in the region where satellite imagery is often affected by clouds.
 2. Regarding the crop yield modeling, the use of annual crop yield data may not be suitable for regions in which multiple cropping systems have been applied. Season-specific or sub-annual crop yield data coincident with the flood event is more appropriate.

Details of these aspects and the framework of this study are presented in the following sections.

3.1. Study framework

As shown in Fig. 3, this study comprises three major parts: 1) crop yield analysis, 2) flood analysis, and 3) vulnerability curve analysis. The crop yield analysis consists mainly of multiple linear regression-based yield modeling using The Moderate Resolution Imaging

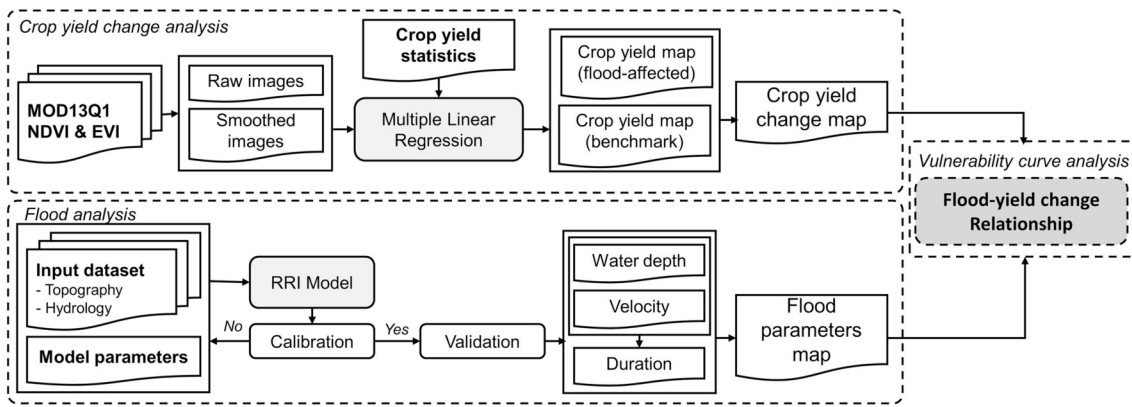


Fig. 3. Study framework adapted from Chen et al. [51].

Spectroradiometer (MODIS) vegetation indices (MOD13Q1) and city-scale crop yield statistics. In this study, multiple NDVI and EVI images based on raw (original) and smoothed images were used as potential predictors for estimating crop yield on a grid-scale. Crop yield change due to flood was estimated using the relative difference between a flood-affected year and a benchmark year [51]. We selected NDVI and EVI as parameters for crop yield estimation because these vegetation indices have been successfully used for yield estimation in the previous studies [52–55]. Moreover, MODIS products are available worldwide in moderate resolution and high acquisition frequency (one or two revisit per day); thus timely spectral information of the instant effect of the flood event can be identified [23,50,56,57]. In the second analysis, flood modeling was used to estimate flood characteristics of the historical flood event in the same grid as the crop yield model. Rainfall-Runoff-Inundation (RRI) model [58] was used to determine the intensity of flood parameters, water depth, velocity, and duration. In the last analysis, we compared the crop yield loss and flood characteristics to derive a relationship. Then, the flood vulnerability curve for rice crop or damage function could be obtained.

3.2. Materials

3.2.1. Crop yield analysis

Data used in the crop yield analysis are shown in Table 1. The Terra MODIS vegetation indices (MOD13Q1) Version 6 at 250 m spatial resolution, obtained from the Land Processes Distributed Active Archive Center (LP DAAC), were used as parameters to estimate the crop yield. We utilized the advantages of the MOD13Q1 product as it has 16-day composite images to obtain cloud-free images, which is preferable for application in cloudy regions i.e., this case study (despite a few missing data and noises) [59–61]. The two primary vegetation indices of MOD13Q1 product, NDVI and EVI, were used in this study from 2006 to

2016. This period was selected to obtain a longer continuous time-series for smoothing (see Material and methods section for detail). Further, two tiles (h28-v09 and h29-v09) were acquired for study coverage.

Rice crop yield statistics obtained from Statistic Indonesia (BPS) were used as dependent variables to build crop yield models in this study. The data used were the first sub-annual statistic for January–April 2008 (hereafter referred to as 2007 yield) and the sub-annual season yield data statistic January–April 2015 (hereafter referred to as 2014 yield). The 2007 yield data covers the harvested yield data for the rainy season affected by the 2007 flood, while the latter was used as a benchmark for calculating the crop yield change in 2007. The 2014 yield is used as a benchmark since it is close to the average of long-term observed historical data.

Land use mask of rice crop in each city-level was used to exclude other land use (non-rice) pixels. The data was provided by the Geospatial Information Agency of Indonesia (BIG). We used the 2010 data for all periods used in this study as there is no significant change of land use within the study area. The masked images were then used to calculate the average value in each city.

For validation, we used total area data statistics of rice crop loss in each city during the period of flood, obtained from the Ministry of Agriculture of Indonesia. We compared the total area of rice crop loss (hectares) between the model estimate and the crop loss statistics for each city.

3.2.2. Flood analysis

The Rainfall-Runoff-Inundation (RRI) model was used to simulate flood characteristics [58]. This model is two-dimensional and can simulate rainfall-runoff and flood inundation simultaneously. Further, it can simulate water depth and discharge in both spatial and temporal scales with the Digital Elevation Model (DEM) and rainfall input data with some other parameters as inputs. The model offers flexibility to set inputs in regard to data limitations, e.g., employing empirical equations to calculate river geometry data which is often sparse and giving evapotranspiration rate, initial and boundary conditions, land use types or soil classes, river diversion, and dam operation scheme as optional inputs [62]. The RRI model does not require a high-resolution terrain model, because it is a grid-based model and any common grid resolution can be used, depending on the purpose of the study. Therefore, the model's application is suitable for developing regions where the most flood-prone crop cultivation areas are often located [63,64].

The governing equations of the RRI flood inundation model are derived based on the mass balance (Eq. (1)) and momentum equations (Eqs. (2) and (3)) for unsteady flow:

$$\frac{\partial h}{\partial t} + \frac{\partial q_x}{\partial x} + \frac{\partial q_y}{\partial y} = r \quad (1)$$

Table 1
List of data used for crop yield estimation.

Data	Resolution	Period	Specification	Source
MOD13Q1 vegetation indices	250 m	2006–2016	h28-v09 tile h29-v09 tile	Land Processes Distributed Active Archive Center (LP DAAC)
Rice crop yield statistics	City-level (17 cities)	2007–2008 2014–2015	Sub-annual data of January–April 2008 & 2015	Statistic Indonesia (BPS)
Land use mask of rice crop	Vector file	2010		Geospatial Information Agency (BIG)
Rice crop loss area	City-level (17 cities)	2007–2008	Total area (hectares)	Ministry of Agriculture

$$\frac{\partial q_x}{\partial t} + \frac{\partial uq_x}{\partial x} + \frac{\partial vq_x}{\partial y} = -gh \frac{\partial H}{\partial x} - \frac{\tau_x}{\rho_w} \quad (2)$$

$$\frac{\partial q_y}{\partial t} + \frac{\partial uq_y}{\partial x} + \frac{\partial vq_y}{\partial y} = -gh \frac{\partial H}{\partial y} - \frac{\tau_y}{\rho_w} \quad (3)$$

where h is the water height from the surface; q_x and q_y are the unit width discharges in the x and y directions, respectively; u and v are the flow velocities in x and y directions, respectively; r is the rainfall intensity; f is the infiltration rate; H is the water height from the datum; ρ_w is the water density; g is the gravitational acceleration; τ_x and τ_y stand for the shear stress in the x and y directions, respectively; t is time. The two-dimensional equations are solved by adopting a diffusive wave approximation. Details on the model structure and its components were explained in Sayama et al. [58].

The input data for the RRI model are shown in Table 2. The model used rasterized topographic information and rainfall as inputs. Precipitation data from 181 rain gauge stations, provided by the Solo river basin organization (BBWSBS), were used for input. The Thiesen polygon was used to generate a spatial distribution of rainfall during the period simulated. The observed daily average river discharges at the Cepu station (Fig. 1), calculated from observations collected three times per day, were used for model calibration. The period of rainfall and river discharge used in this study was from January 1, 2007 to January 31, 2008.

A Digital Elevation Model (DEM) HydroSHEDS 3 was used to represent the surface topographical characteristics of the basin [65]. The DEM was provided by the United States Geological Survey (USGS) with 3 arc second or ~ 90 m resolution (at the equator) as the finest resolution. In this study, the 30 arc-second and 3 arc-second resolutions were used for model fitting and application, respectively. The 3 arc-second resolution was then resampled to 250 m, consistent with the MODIS-based crop yield model. DEM was used to delineate the catchment area and derive the flow accumulation and direction; the latter were used to identify river and slope cells as the main input for the RRI model. For validation, we used an inundation extent within the flood period that was mainly derived from the Dartmouth Flood Observatory map and various remote sensing data (Table S2, Supplementary Data).

3.3. Methods

3.3.1. Crop yield analysis

The MOD13Q1 of the two tiles h28-v09 and h29-v09 that cover the

Table 2
List of data used for flood simulation.

Data	Parameters	Resolution	Source	Data period
Topography data	DEM, flow direction, and accumulation	3 arc-second (~90 m) resampled to 250 m MODIS resolution	HydroSHEDS United States Geological Survey (USGS)	–
Gauged rainfall	Daily rainfall (mm)	Daily data of 181 stations	The Solo river basin organization (BBWSBS)	January 1, 2007–January 31, 2008
Observed river discharge	Daily mean discharge (m^3/s)	Daily averaged data of one station (Cepu station)	BBWSBS	January 1, 2007–January 31, 2008
Other remote sensing data	Flood extent	(Table S2, Supplementary Data)		

study area were downloaded, mosaicked, projected to the geographic coordinate system, and stacked in time series. Then, two types of inputs were prepared: 1) raw and 2) smoothed images. The original NDVI and EVI layers directly acquired were considered as raw images. As the first type of input, raw images were used to preserve original characteristics of the time series profiles that are due to some variations including plant stress and inundation [23,50,66]. It can be useful for developing the model to capture the impact of the flood on rice crop from this study, as it is sensitive to such stress [23,67].

However, the drawbacks of using raw values from optical imagery such as MODIS consists in the presence of optical noises and cloud coverage especially during the rainy season, which is the target period of this study. Therefore, as the second type of input, we used smoothed images [68,69]. These images were pre-processed images in which noises in the phenological time series were removed and interpolated. The interpolation was done by the Savitzky–Golay filter performed by TIMESAT [70]. The pixel reliability layer was used for weighting each NDVI and EVI observation value and bad quality pixels were set to NA. Tuning filter parameters was done by visual interpretation using the user interface (see Eklundh and Jönsson [70] for details).

As shown in Fig. 4, the big flood event period in late December 2007 occurred during the rainy season paddy cultivation (green shade). In this study, two periods (2007 and 2014) of the first rainy rice-growing season (usually starting in October) were chosen for estimating the crop yield change during the 2007 flood event. We used a specific season yield rather than annual yield, to isolate the flood impact and exclude biases from the impact of the other seasons of the same year. For instance, higher yield in the dry season compensating the low yield in the flood season can affect the average value of annual yield. The yield data for 2007 and 2014 in the city level is shown in the Supplementary Data (Table S1). It shows that the yield value for the 2007 first rainy season was relatively lower than the 2014 season. It allowed us to obtain losses from comparing these two-year data with the assumption that no other major causes affected the losses during the season.

Raw and smoothed time series of NDVI and EVI were then masked in each city-level rice crop area. The land use in 2010 was used in this study. Although the land use might change over time, we observed no significant change of land use within the study area, since the average change of the paddy field area in most of the cities in the basin was less than 0.5%. Then, the raw and smoothed NDVI and EVI layer stacks were used to calculate the average value based on the city mask to represent the indices within the city, since the yield statistic is based on the city-level.

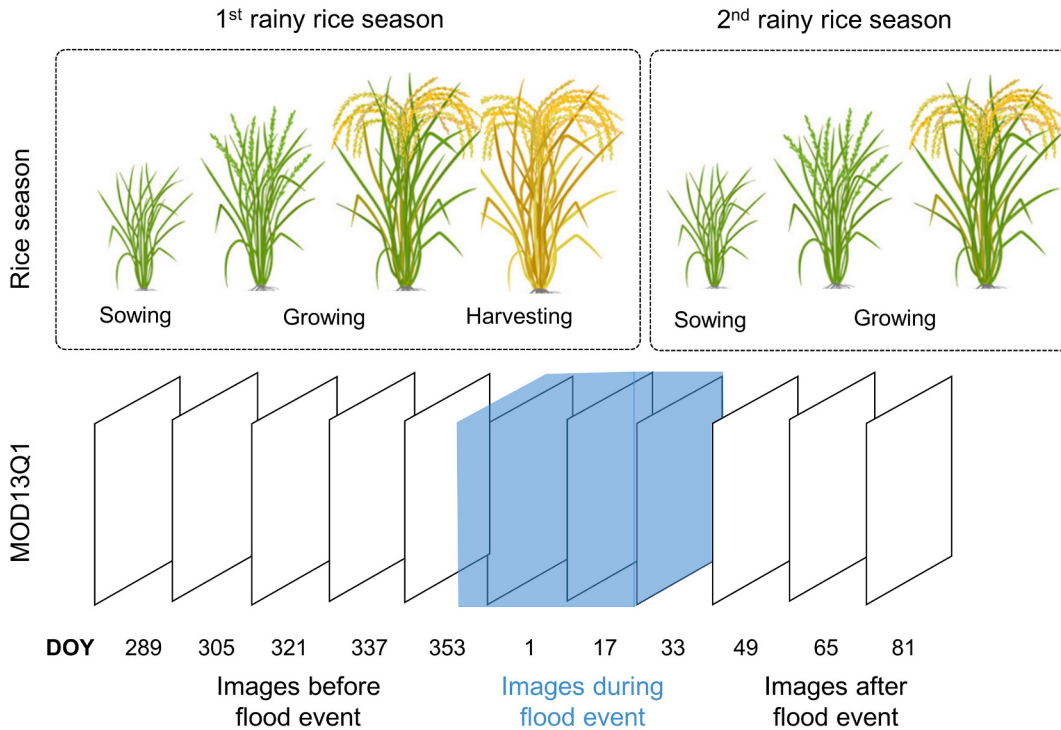
We used multiple linear regression with average NDVI and EVI as predictors and yield data statistics as dependent variables, in a city-level as shown in Table S1 (Supplementary Data). Models were derived based on 17 administrative cities located in the river basin (Fig. 1). Two regression models were built for years 2007 and 2014, respectively. The selection of the most relevant predictors was done using a stepwise approach with 95% confidence level [51,71,72]. The window of potential predictors was selected during the first rainy crop season which occurred from October until March. Associated with MODIS data retrieval, NDVI, and EVI of Day of Year (DOY) 289 (16 October) until DOY 81 (22 March) of the following year were used for 2007 and 2014, respectively (Fig. 5). In addition, we considered NDVI and EVI images which were close to the heading phase. A previous study by Son et al. [54] suggested that there is a higher correlation between NDVI and EVI profile and yield during the heading stage and between sowing and harvesting, shown by the phenology signal. Once the selected NDVI and EVI values were paired with the city level yield data, a regression analysis was carried out using Eq. (4).

$$Y = \beta_0 + \beta_1 X_1 + \beta_2 X_2 + \dots + \beta_n X_n \quad (4)$$

where Y is the estimated yield of rice crops (tons/ha), β_0 is the model intercept, β_n is the regression coefficient, and X_n is NDVI and/or EVI with

Year	2007 / 2014								2008 / 2015			
Month	May	Jun	Jul	Aug	Sep	Oct	Nov	Dec	Jan	Feb	Mar	Apr
Agricultural statistic	2 nd Sub-annual data				3 rd Sub-annual data				1 st Sub-annual data			
Crop season used in this study												

Sowing Growing Harvesting
Flood period

Fig. 4. Crop statistic retrieval period and targeted season.**Fig. 5.** Affected rice season, The Moderate Resolution Imaging Spectroradiometer (MODIS) images frequency, and flood event periods.

index n of DOY used during crop growing season.

After the regression models were applied, we used Eq. (5) to estimate the yield change due to the 2007 flood as an expression of relative change. From Eq. (5), a crop yield change with a negative value is considered as "yield loss," which means that the yield in 2007 was lower than in 2014 as a normal year; a crop yield change with positive value was considered as "yield gain" for 2007 during the flood period.

$$\text{Crop yield change} = \frac{\text{Yield}_{2007} - \text{Yield}_{2014}}{\text{Yield}_{2014}} \times 100\% \quad (5)$$

where Yield_{2007} is the rice crop yield in 2007 (tons/ha) during the harvesting period of the first rainy rice season, and Yield_{2014} is the rice crop yield in 2014 as a benchmark year (tons/ha).

3.3.2. Flood analysis

The model parameters were calibrated by fitting simulated and observed river discharges in the Cepu observation station during the late 2007 flood event (December 23, 2007–January 17, 2008). The model fitting was done by running a model with the coarser 30 arc-second resolution topographic data, and then applying the fitted parameters to the finer 250 m resolution data, for study application. We used a single land use with the Green-Ampt model scheme; the topographical conditions of the case study are mainly plain areas where infiltration excess of overland flow is dominant. In addition, we used references from Kudo et al. [73], which conducted the same case study using the

same model (RRI model).

According to Sayama et al. [58], determining model parameters can be done by a trial-and-error approach. In this study, the model parameters fitted were limited to the Manning coefficient for slope (n_s), while the Manning coefficient for the river (n_r) was set to 0.03. The parameter n_s was determined by testing several values: 0.06, 0.08, 0.1, 0.12, and 0.2, and following the ranges that have been used by previous model applications [73,74]. The Green-Ampt model parameters were set based on the silt loam soil texture, as shown in Table 3. Lateral subsurface flows, groundwater, and evapotranspiration were not calculated in the simulation. For the river channel geometry, we used a simple regression equation [58,62], since the river cross-section data was not available in the study area as width = $C_w A^{Sw}$ and depth = $C_d A^{Sd}$, where A is the area of its catchment and C_w , Sw , C_d , and Sd are the regression parameters which were set to 5.0, 0.35, 1.2, and 0.2, respectively.

The extended simulation was conducted for the period of January 1, 2007 to January 31, 2008. There were 734,371 grids (1111 × 661) of

Table 3
Green-Ampt parameter input in the RRI model.

Input parameters	Value
Soil depth	1 m
Vertical hydraulic conductivity (k_v)	0.68 cm/h
Porosity (φ)	0.501
Capillary head (S_f)	16.68 cm

input and output raster files. The model output for depth and discharge in the river and the slope were set to daily, consistent with the observed discharge data (396 files over 396 days of the simulation).

The operation of the Wonogiri dam was also considered in this study, with its $220 \times 10^6 \text{ m}^3$ of flood control storage capacity. Similar to Kudo et al. [73], the constant outflow discharge was set to $400 \text{ m}^3/\text{s}$ when the inflow exceeds this value. When the dam's storage exceeds the flood control storage capacity, the dam's outflow was set to the same value as the inflow.

The output parameters used in this study are water depth (m), velocity (m/s), and duration (days). The velocity was derived from the discharge on a unit of area of each pixel; the duration was obtained by accumulating the total inundation period of the flood. It should be noted that the duration does not represent the duration of consecutive inundation. The flood duration refers to the duration of water inundation of the soil's surface, rather than the duration of submersion or water-logging in the soil before and after a flood event, which also may affect plants.

3.3.3. Vulnerability curve analysis

We used maximum depth, maximum velocity, and maximum duration as a representation of the flood parameters. The maximum depth and velocity represent the peak intensity of depth and velocity during the flood simulation, and the duration represents the total accumulation of inundation periods during the flood event used in this study (December 23, 2007–January 17, 2008). We investigated the relationship by scatter plots with the x-axis set as the intensity of the flood parameters (maximum depth, velocity, and duration) and y-axis as the degree of yield loss. Then, we obtained the vulnerability curve from this relationship.

As we have paired crop yield and flood model output aligned with the same resolution, we could directly compare them and derive a relationship. However, due to the huge number of pixels, we used a discretization method to sort data values into a number of bins, called binning [75]. Adopting the previous study [51], we partitioned all values within pixels into equal-intervals of every 0.01 or 1% relative change of crop yield. Then the pixels distributed in a bin were used as a mask, to extract an average value of the flood parameter (e.g., for the range of 0–75%, there would be 75 bins).

3.3.4. Model evaluation

Regarding the model fitting process for crop yield and flood model, we assessed the comparison between simulated and observed data using the simple parameter R^2 , percent error (%), and The Nash–Sutcliffe model efficiency coefficient (NSE) [76].

For validating the flood inundation extent, we used a simple comparison between the simulated data and the observed inundation obtained by remote sensing imagery, called coincidence extent [58,77] or fit index [64,77]. We obtained a satellite image in the available period of temporal frequency, around the peak of the flooding time during the flood event, and then compared it with the simulated inundation of the same period it was retrieved. The result was evaluated with:

$$F = \frac{A_s \cap A_o}{A_s \cup A_o} \quad (6)$$

where $A_s \cap A_o$ is the intersection between simulated and observed flood inundation extent, $A_s \cup A_o$ is the union of those extents, and F is the fit index of inundation extent. The larger F indicates more coincidence between simulated and observed flood inundation extent.

4. Result

4.1. Crop yield analysis

4.1.1. Crop yield model

Based on the stepwise approach in the regression analysis, the parameters and equations shown in Table 4 were selected as models to derive crop yield maps. The calibrated model performs in moderate agreement with, respectively, 0.52, 0.45 and 0.61, 0.59 for the R^2 and adjusted R^2 of the 2007 and 2014 model. The p-value shows that relationships are significant, with 0.006 and 0.0002 of the p-value for both models, respectively. The selected variables in the regression equations are the raw value of NDVI of December 3, 2007 and EVI of January 17, 2008 for the 2007 model. For the 2014 model, we selected the raw value of NDVI on March 22, 2015. In this study, the raw values of NDVI and EVI are considered suitable predictors, rather than their smoothed values. This reveals the significance of raw values to estimate the yield in a city-scale, being sensitive to short variations such as floods. In particular, the flood-affected year model accounts for predictors value in the vicinity of the flood event period (EVI of January 17, 2008). The use of predictors during or immediately after the flood event can give the flooding spectral influence in the regression-based model as NDVI and EVI would give a significantly lower value when the land is flooded by water. In addition, the use of raw values is favorable for retaining the original characteristics of the surface reflectance. It can account for short temporal variation due to flooding.

The comparison between observed yield and model, showing that both models are close to the 1:1 line (Fig. 6). Moreover, the 2007 yields are lower than those of 2014. The low values of 2007 represent the disruptions in yield due to any factors, including the flood. Since the yield data were from rainy season cultivation, rice crop was likely disrupted by the flood, instead of droughts. The droughts usually occur during dry seasons, which was beyond the temporal window of this analysis.

4.1.2. Map of crop yield change

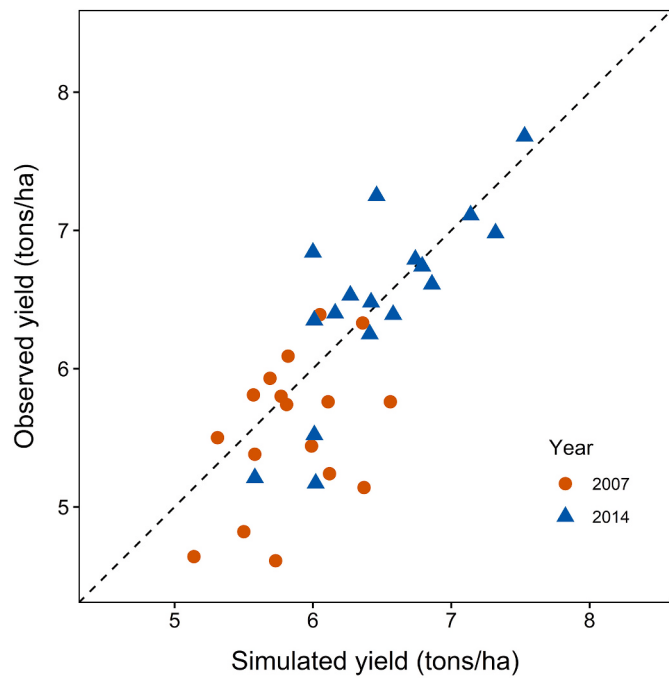
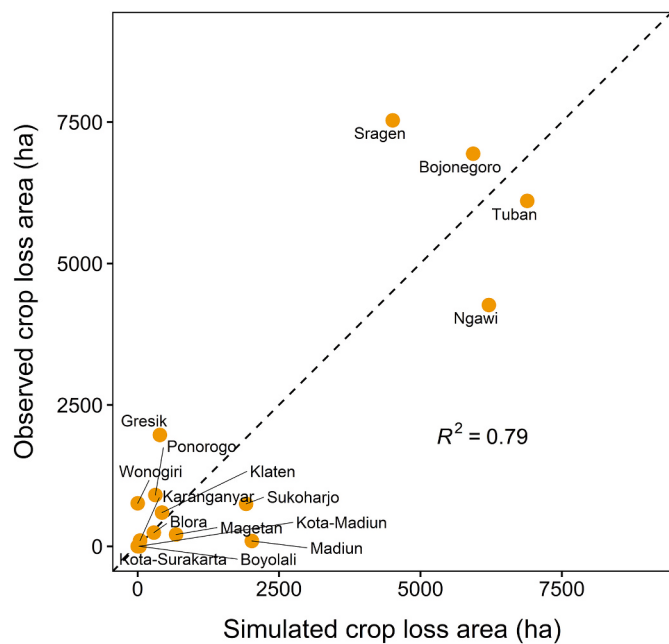
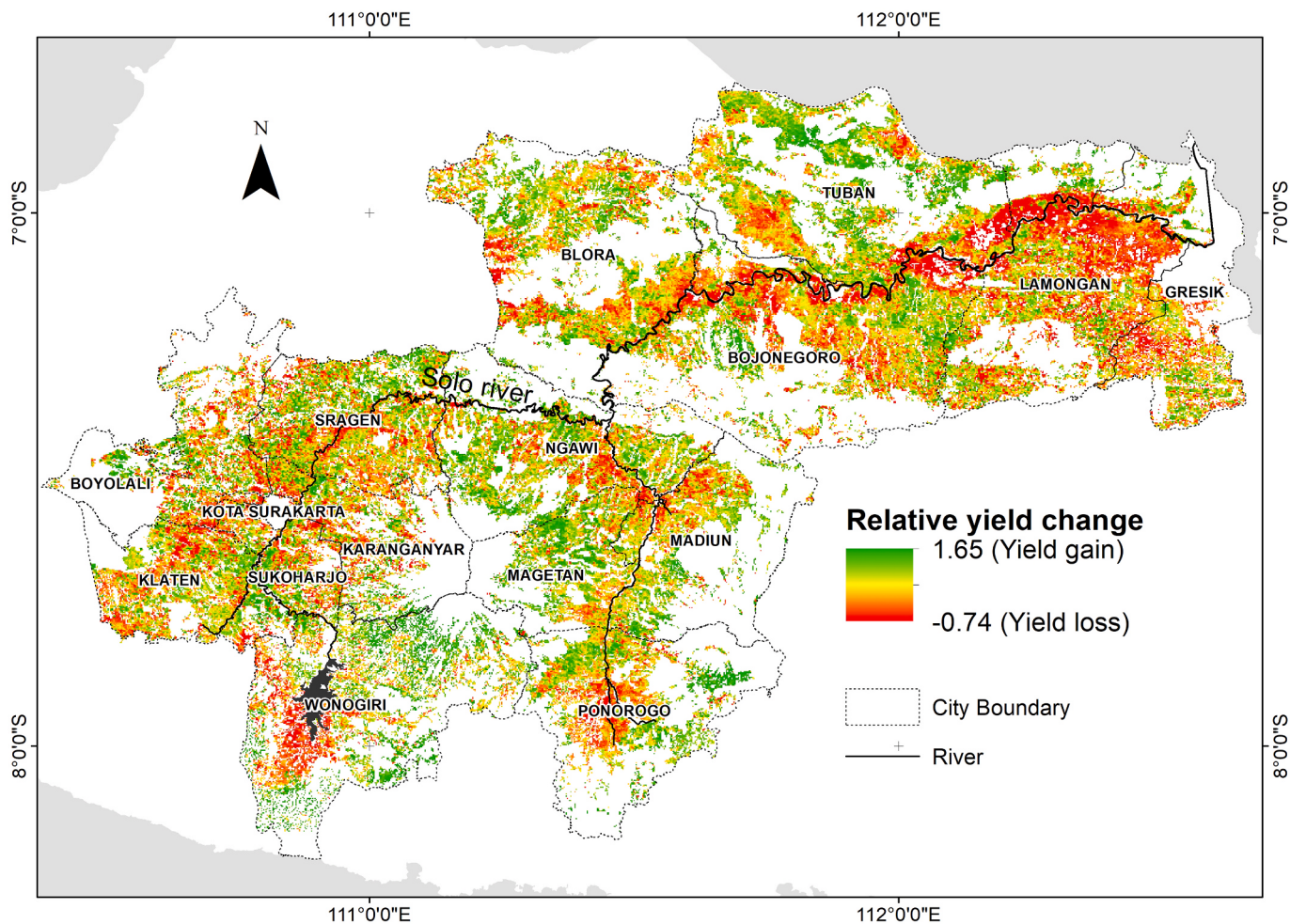
As seen in Fig. 7, the crop yield change between 2007 and 2014, obtained with Eq. (5), shows a robust signal of flooding stress (yield loss) indicated by the negative value of yield change in the flood-prone area that lies downstream of the river; yield loss pixels apart from the river are also observed. The possible reason for this is that there were many causes that influence the VI spectral of the crop in the field (e.g., different rice crop growth stages) which, in turn, affected the yield value in pixels (e.g., the signal from water ponding during a transplantation stage of paddy).

To validate this model, we compared the rice crop loss area based on pixels with the observed total crop loss area due to the 2007 flood event, based on the city-scale statistics provided by the Ministry of Agriculture of Indonesia. We compared the observed total crop loss area (hectares) with the crop loss area obtained by simulation, in every city (Fig. 8). The result shows that the simulation is in good agreement with the observation ($R^2 = 0.79$). However, it should be noted that this comparison does not reflect the pixel-wise coincidence between simulated and observed loss area distributions, since observed data is only an accumulated value without information on spatial distribution within each city.

Table 4

The regression equations for crop yield estimation.

Model	Regression equation	p-value	R^2	Adj. R^2
2007–2008 (Raw images)	$Y = 6.860 - 5.624 \text{ NDVI}_{3\text{Dec}07} + 3.478 \text{ EVI}_{17\text{Jan}08}$	0.006	0.52	0.45
2014–2015 (Raw images)	$Y = 10.83 - 7.651 \text{ NDVI}_{22\text{Mar}15}$	0.000	0.61	0.59

**Fig. 6.** Observed and simulated city-scale rice crop yield.**Fig. 8.** Observed and simulated city-scale rice crop loss area during the 2007 flood.**Fig. 7.** Crop yield change between 2007 and 2014.

In Fig. 8 it can be seen that there was a higher crop loss area in several cities located in the middle valley, toward the downstream of the river basin (e.g., Ngawi, Tuban, Bojonegoro, Sragen, Lamongan). However, Lamongan city data was not included in the relationship shown in Fig. 8, since we obtained a large discrepancy between the simulated and observed crop loss area in this case. It has been reported that rice crop areas in Lamongan city mostly changed to fishpond during the rainy season. Therefore, similar land use masks could not be used, and most of the crop loss grids simulated in Lamongan city might be false positive.

4.2. Flood analysis

4.2.1. Model calibration

The evaluation results of parameter fitting are shown in Table 5. A better agreement, indicated by the maximum value of the NSE (0.912) and the minimum value of the percent error in peak discharge (PEP) (-4.06%), was obtained when the Manning coefficient of the slope (n_s) was 0.1. The PEP was calculated by dividing the difference between the simulated and observed peak discharge by observed peak discharge on December 29, 2007 ($3324.41 \text{ m}^3/\text{s}$), expressed in a percentage; the negative PEP value represents underestimated simulated discharge. According to Moriasi et al. [78], these values of NSE and PEP indicate that the model simulation was in a very good performance ($0.75 < \text{NSE} < 1.00$ and $\text{PEP} < \pm 10\%$). Therefore, considering both NSE and PEP, we chose a parameter set with $n_s = 0.1$ for the calibrated model. These parameter value can be considered representative, as Chow [79] provided a range of Manning roughness coefficients for natural stream channels from 0.03 (clean, straight stream) to 0.1 (with heavy brush and timber), and of flood plains from 0.035 (pasture) to 0.1 (dense trees).

Moreover, simulated flood hydrograph using $n_s = 0.1$ is compared with observed discharge in the Cepu station, as shown in Fig. 9. The simulated hydrograph matches the trend of the observed hydrograph. The comparison between the observed and simulated discharges follow the 1:1 line, indicating that the simulated discharge fits adequately with the observation.

4.2.2. Model validation

The validation of the flood simulation developed in this study was done by comparing the spatial extent of the simulated and observed flood inundation. The simulated inundation extent was obtained using the calibrated parameter with a 250 m grid resolution. Pixels with depth of more than 0.5 m were considered wet pixels. This threshold can be used for comparison with the inundated extent obtained from remote sensing observation [74]. The observed flood extent in this study was based on the remote sensing images retrieved from several satellite image sources (Table S2, Supplementary Data). The wet pixels were classified by adjusting the threshold with a reference from the reported flood inundation extent provided by the Dartmouth Flood map retrieved on December 27, 2007. The overlay between the simulated and observed inundation extent indicates that the simulated inundated area is in agreement with satellite images, especially in the downstream area where a large inundation occurred (Fig. 10). However, the inundation

extent in the middle river reach is significantly discrepant where the simulated inundation area is overestimated.

To assess the agreement between simulated and observed flood inundation extent quantitatively, we evaluated the fit index using Eq. (6). To derive the simulated and observed flood inundation extent, we calculated the total area of each inundation extent in km^2 (Table 6). The total area is based on multiplication of the total number of grids and the average grid size in the geographic coordinate system.

As seen in Table 6, the fit index result shows moderate agreement compared to previous studies using the same model [58,64,74]. This might be due to several factors, as follows. First, the aggregation of the grid spatial resolution from 90 m to 250 m might induce a significant change of the floodplain topographic characteristic. This will affect especially the wide plain area in the middle river reach, where an extensive flood inundation was simulated. Second, the model does not incorporate detailed river cross-section input data and the river channel geometry was simplified using a regression equation [58,62]. Third, the differences might be due to misclassified wet pixels, because the cultivation ponding water in the paddy field looks similar to the riverine flood inundation. Thus, some false positive pixels that refer to the non-flooded pixels are incorrectly classified as floodwater in the remote sensing-based observed flood inundation.

4.2.3. Flood parameter

Flood characteristics were obtained based on the calibrated model applied to the 250 m resolution. The spatial distributions of the maximum depth, velocity, and duration in the flood plain are shown in Fig. 11. Based on the simulation results, a huge inundation area occurred in the downstream area, where rice crop fields were massively cultivated. The maximum depth, velocity, and duration within all the inundated pixels is 4.44 m, 0.5 m/s, and 25 days, respectively. These three flood parameters were used to obtain a relationship between flood and crop loss.

4.3. Vulnerability curve analysis

4.3.1. Flood and crop yield change relationship

The intensity of flood parameters and the degree of yield change relationships are shown in Fig. 12. The relationships show that the x-axis divides two quadrants of the crop yield change value: the first contains the positive values of yield change that indicate the yield gain in 2007, and the second, the negative value of yield change that indicates the yield loss. The transition from the yield gain (crop yield change < 0) to the yield loss (crop yield change > 0) crossing on the x-axis is considered as minimum damageable values, where flood parameters start to induce damage to the rice crop. For water depth, flow velocity, and duration relationship, as shown in Fig. 12(a), (b), and 12(c), the minimum damaging values are 0.2 m, 0.03 m/s, and 8 days, respectively. Furthermore, considering the yield gains shown by the positive crop yield change value, these results reveal - to a certain degree - the positive impact of the lower magnitude of the flood. As pointed out by previous studies [36,37], rice crops can grow well in wet fields and are highly tolerant to excess water stress arising from flooding. However, the depth, velocity, and duration relationship uncertainty becomes increasingly larger as the curve enters the yield change's positive values, or yield gain zone, shown by a larger range of the 95% confidence interval.

In addition, it should be noted that each flood parameter (depth, velocity, and duration) of the relationships are not associated with other flood parameters. For example, previous studies combined depth and duration to get a relationship with crop yield loss [29,31,32,38]. Due to its limitations, the crop yield change in this study corresponds only to one flood parameter independently, instead. For instance, the duration or the depth parameters used to obtain the relationship are not associated with a specific boundary of the flood depth or duration conditions.

Furthermore, it should be noted that, in the case of velocity and

Table 5
Evaluation of the simulated discharge based on different Manning coefficient of the slope (n_s) used in the model calibration.

Manning coefficient	$n_s = 0.06$	$n_s = 0.08$	$n_s = 0.1$	$n_s = 0.12$	$n_s = 0.2$
NSE	0.906	0.898	0.912	0.910	0.911
Peak discharge (m^3/s)	3156.34	3187.19	3189.5	3185.36	3181.51
Percent error in peak discharge (PEP) (%)	(-5.05%)	(-4.13%)	(-4.06%)	(-4.18%)	(-4.30%)

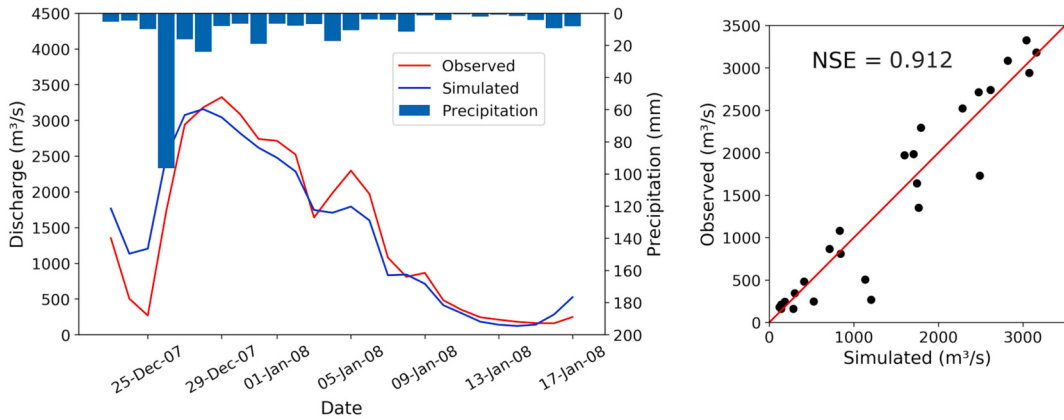


Fig. 9. Observed and simulated river discharge at the Cepu Station during the 2007 flood.

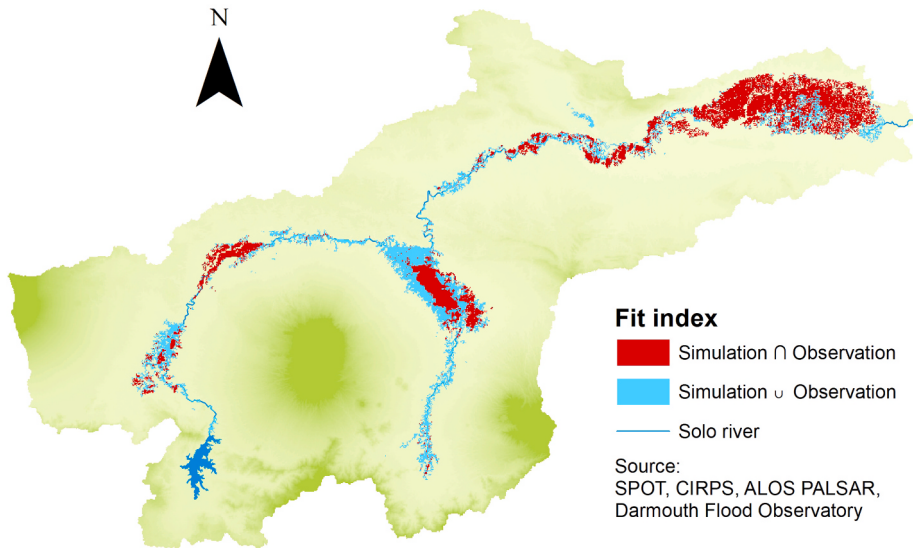


Fig. 10. Simulated and observed flood inundation extent using the RRI model and based on satellite images respectively.

Table 6

The fit index (F) between peak simulated and observed inundation extent.

Total area (km^2)		F
$A_s \cap A_o$	$A_s \cup A_o$	
667.1 km^2	1601.2 km^2	0.42

duration relationships, we omitted some of the pixels with values less than the minimum damageable depth that was revealed based on the depth-loss relationship (Fig. 12(a)). As mentioned, the minimum damageable depth obtained in this study is 0.2 m. Based on our assumption, this threshold was necessary to mask out some pixels and thus avoid significantly small values that do not impact the crop.

4.3.2. Vulnerability curve

We constructed vulnerability curves from the relationships between the intensity of flood parameters and the degree of yield loss shown in Fig. 13. In the vulnerability curve metric, the y-axis is usually represented by a fraction of a loss or damage component (0–100%). It should be noted that the loss component is defined here by crop yield loss; the other damage components (e.g., production, harvest area) resulting from the adverse impact of the flood are outside of this study's scope.

The flood depth-loss relationship shown in Fig. 13 (a) illustrates a negative impact of the flood on the crop yield. Higher intensity of the

flood depth brings higher yield loss, shown by the decrease of the yield of 2007, relative to 2014. The water depth of 0.2 m (minimum damageable depth) starts to induce loss. Moreover, Given the nature of the paddy fields grown in semi-aquatic environment, Rowshon et al. [80] confirmed that ~5–10 cm ponding water is maintained throughout most of the growing season. Subsequently, 0.2 m can be regarded as close to the “tolerable” water depth. Moreover, by taking into account that plant height during maturity stage is 1 m, when rice plants are completely submerged a damage of ~50% can be still maintained. The possible argument here is that the rice crop can survive within wet stress conditions by employing a tolerance mechanism [2,6,7,36,37]. Therefore, the crop might withstand the flood, even if completely submerged. Furthermore, using the regression equation shown in Table 7, maximum damage is reached when the water depth is 5.2 m. Nonetheless, as mentioned, this depth value does not correspond to any inundation duration, being independently represented by one parameter solely. In fact, lower depth with longer duration may intensify the level of damage in the associated growth stage, resulting even in complete damage [30, 31].

The flood velocity-loss relationship exhibits a 0.03 m/s minimum damageable flow velocity (Fig. 13 (b)). Moreover, based on the regression equation shown in Table 7, a maximum damage of 100% would likely be attained when the velocity reaches 0.08 m/s (maximum damageable velocity). Given the gentle characteristics of the Solo river basin, our flood modeling reveals a lower velocity, in contrast to flash

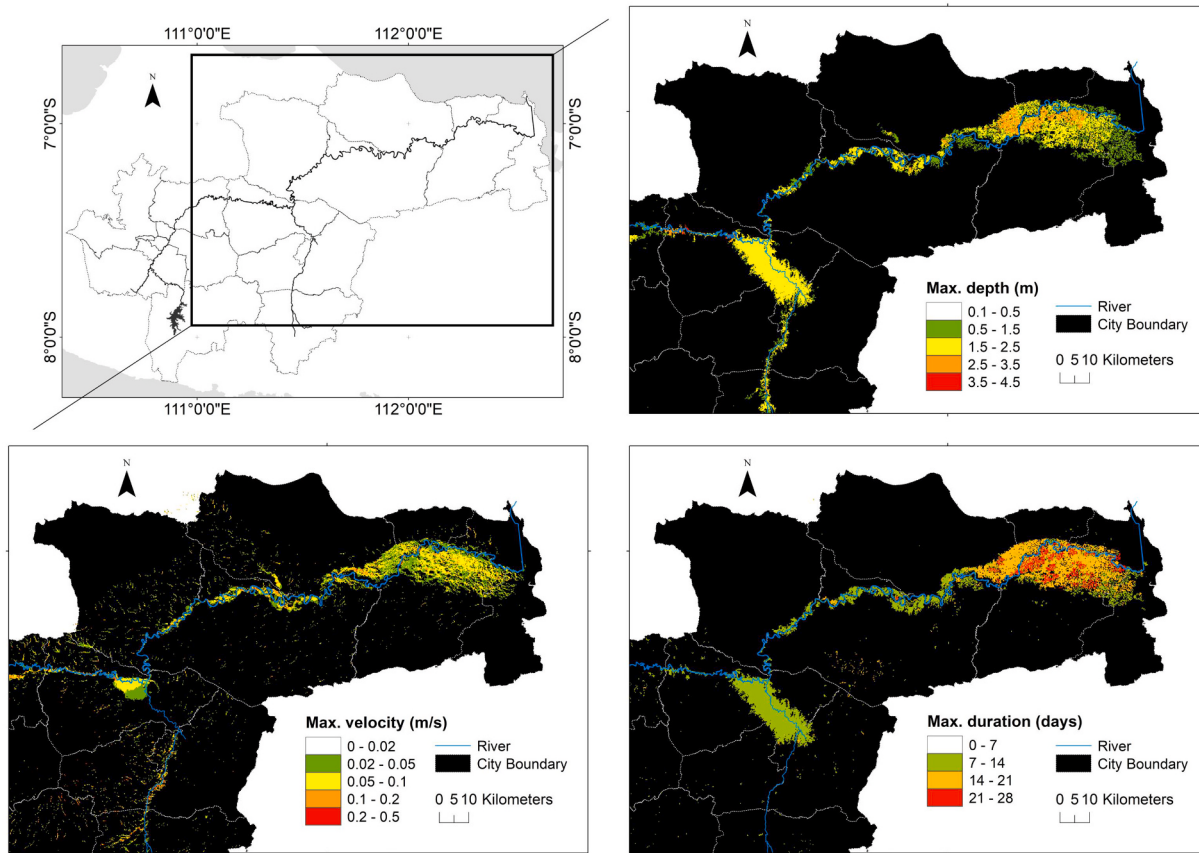


Fig. 11. Simulated flood parameter map using the RRI model.

flood cases.

The flood duration-loss relationship (Fig. 13 (c)) shows a minimum damageable flood duration of 8 days. Using the regression equation shown in Table 7, 100% or complete damage of the rice crop would likely be achieved by 22 days of inundation. This result seems overestimated, compared to previous studies in the field of plant physiology [81–83]. However, this finding is comparable with previous studies of flood-tolerant rice. With the introgression of SUB1 gene, it was reported that flood-tolerant rice could withstand floods of up to ~14–17 days [6, 7,83–85]. Nevertheless, because the duration parameter used in this relationship does not correspond with any water depth condition, even 24 days of inundation might not induce severe damage to the rice crop, if associated with very shallow depth.

The relationships of each flood parameter and the degree of yield loss show that flood hazards result, generally, in a negative impact on the crop yield, with logarithmic function relationships. The function obtained from all these relationships shows good reliability with R^2 of 0.98, 0.71, and 0.83 for depth, velocity, and duration relationship, respectively. To predict yield loss using these study results, these functions may be suitable for use and testing of other case studies, with input given by the standard flood parameter obtained from any hydrodynamic model.

5. Discussion

This study reveals that water depth is the most significant parameter, as pointed out in previous studies [23,24]. Here, we discuss the comparison among several previous studies that explicitly used flood depth as flood parameter in their flood vulnerability curves for rice crop. Table 8 shows a summary of these studies, while the graphical comparison among six studies that use similar vulnerability matrices is shown in Fig. 14. It should be noted that these studies vary, in terms of

what they consider as conditions, between seasonality (e.g., vegetative, reproductive, and maturity stage) and flood duration. Some studies even include both seasonality and duration, combined with the depth parameter [30–32]. Here, we selected one of the vulnerability curves associated with a generally longer inundation period (e.g., 14 days) that occurred when the crop was at maturity growth stage, if several types of vulnerability curves associated with the above parameters were provided.

In terms of curve slope and damageable depth threshold, these six studies exhibited two different types of vulnerability curves, generally. The first group contained vulnerability curves with a relatively steep slope and shallower maximum damageable depth inducing a complete or 100% crop loss [31,40,56]. This group of vulnerability curves is mostly obtained based on empirical data, and expert and farmer's knowledge. These types of curves proposed a minimum damageable depth of 0.3–0.5 m, and a maximum damageable depth of 1–1.5 m at specific crop growth stages and flood duration (Table 8). Representing this group, Shrestha et al. [31] considered that damage will occur at a specific minimum damageable depth (i.e., 0.2–0.5). While the complete damage will occur at the maximum damageable depth of 10 cm below the average plant height (e.g., 10 cm below 1.3 m - the rice plant height at ripening stage). Given a similar range of damageable depths, this group of vulnerability curves is strongly associated with the nature of rice plant height at specific crop growth seasons.

The second group contains vulnerability curves with a relatively less steep slope and higher maximum damageable depth [32,86]. These curves are obtained from and statistical methods based on farmer's knowledge [32] and literature studies [86]. These types of vulnerability curves show minimum damageable depth mostly by zero water depth, while the range from the minimum to the maximum damageable depth is quite large (3.4–6 m). Huizinga et al. [86] obtained the vulnerability using the average of several regional vulnerability curves from Asia, i.e.,

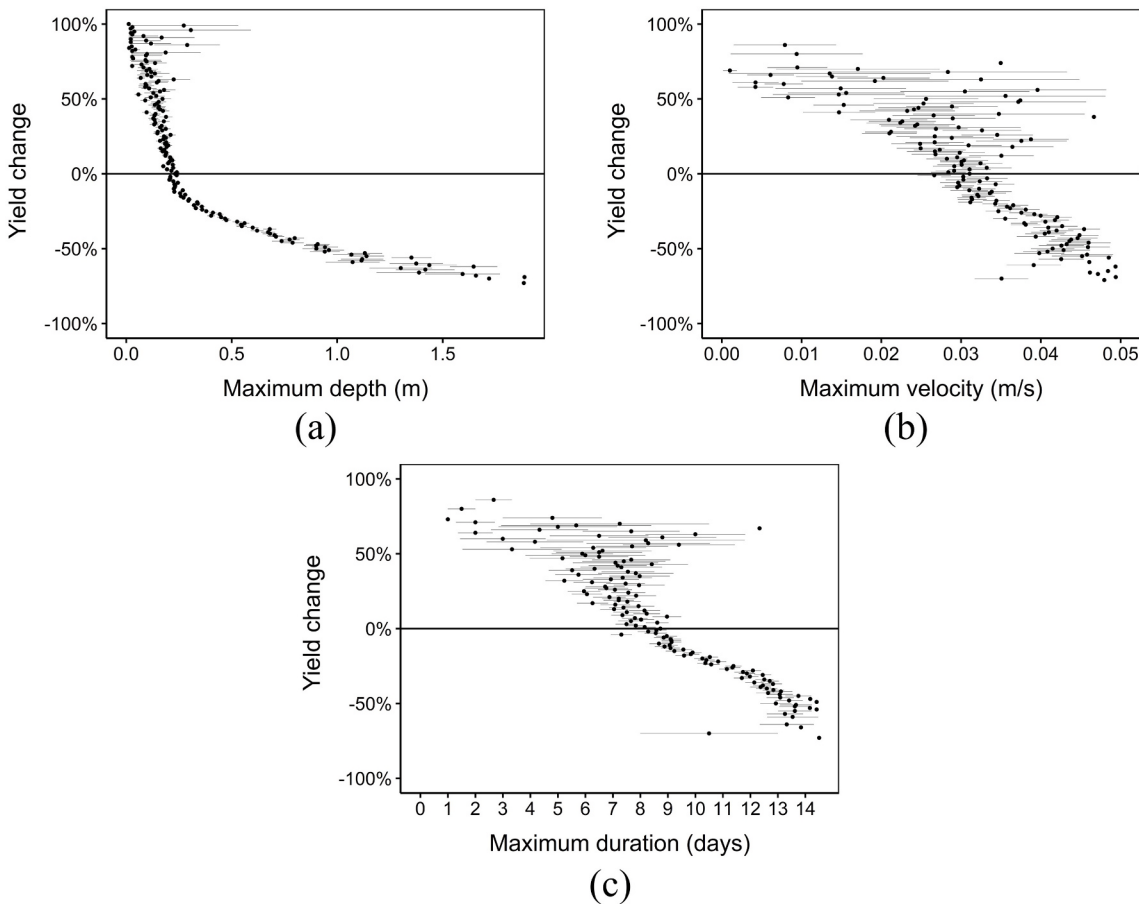


Fig. 12. Relationship between the intensity of flood parameters and the degree of crop yield change. The horizontal tails denote the 95% confidence interval.

Cambodia, Bangladesh, and India. However, the maximum damageable depth in Huizinga's study seems much larger than that reported by others, as they set the maximum damageable depth at 6 m for all sectors (e.g., infrastructure, agriculture) for providing a standardized vulnerability curve in global scale. Moreover, Win et al. [32] and this present study proposed a statistical approach to obtain the vulnerability curves. Win's study used a multiple regression model based on flood duration, depth, and crop growth stage parameters. Given the method to obtain the vulnerability curve, the second group strongly depends on the data and assumptions in their statistical approach. Further, the second group of vulnerability curves does not represent explicitly physical factors, as the first group of studies does. This study's results are considered to be included in this second group of vulnerability curves.

This study also addresses the applicability of the approach proposed by Chen et al. [51] to derive a relationship between flood intensity and the degree of yield loss using integrated crop yield and flood models. We used a similar method (with additional approaches to improve the model), but reached a quite different conclusion in terms of which flood parameter is the most influential in the case of rice. They concluded that flow velocity is the most influential parameter, compared to depth and duration, for all crops, including rice. As they used steep mountainous regions with steep terrains as case studies, it is quite reasonable that flow velocity is considered as most influential parameter, because high flow velocity becomes dominant in the case of flash floods [33]. However, in this study, we studied a case occurring in the Solo river basin, which has a gentle slope characteristic and wide flood plain in most parts. Therefore, flow velocity is not considered as influential as depth and duration.

Moreover, we validated both the crop yield and flood models, confirming that the models' outputs agree with the observed data. However, regarding the crop yield model, the validation could not be carried out in

the explicit grid scale. The spatial variation of yield in the grid-scale may not represent the actual spatial variation and distribution of the yield within a city, because the variation of crop yield loss due to flood in spatial scale is highly dependent on the behavior of NDVI and EVI predictors. Similar attempts have been made by Mkhabela et al. [53]; they validated the crop yields model output using the Census Agricultural Region in Canadian Prairies. Most of the previous studies validated the aggregation of crop loss in administrative levels, because the data from affected fields are quite scarce [22]. Therefore, validating the crop yield model in grid-scale is a substantial achievement for future efforts.

Furthermore, the crop yield model depends on the selection of specific images of MODIS NDVI and EVI as predictors, based on the stepwise approach. Our results show that models derived from images taken during and after the flood event modeled better the flood-affected crop yield map of year 2007 (NDVI in December 3, 2007 and EVI in January 17, 2008), which is in agreement with previous studies [50,56,57,67]. However, when other VIs are used as model predictors, or other case studies are applied, the selected images can be changed correspondingly based on the regression analysis.

More empirical studies can be done on the use of other VIs (e.g., Soil-adjusted Vegetation Index (SAVI) [87], Ratio Vegetation Index (RVI) [88], Leaf Area Index (LAI), Vegetation Health Index (VHI) [89], Vegetation Condition Index (VCI) [90], Disaster Vegetation Damage Index (DVDI) [91], etc.), complementing this study findings. In this study, we used VIs derived directly from remote sensing bands (i.e., NDVI, EVI) rather than derived VIs from other VIs, to avoid determining additional parameters or assumptions (e.g., weight for VHI [92] and adjusting parameters for SAVI and OSAVI), which are sensitive to the results. Moreover, the impact of VI changes during critical growing period and flood event is more important to capture the crop yield loss

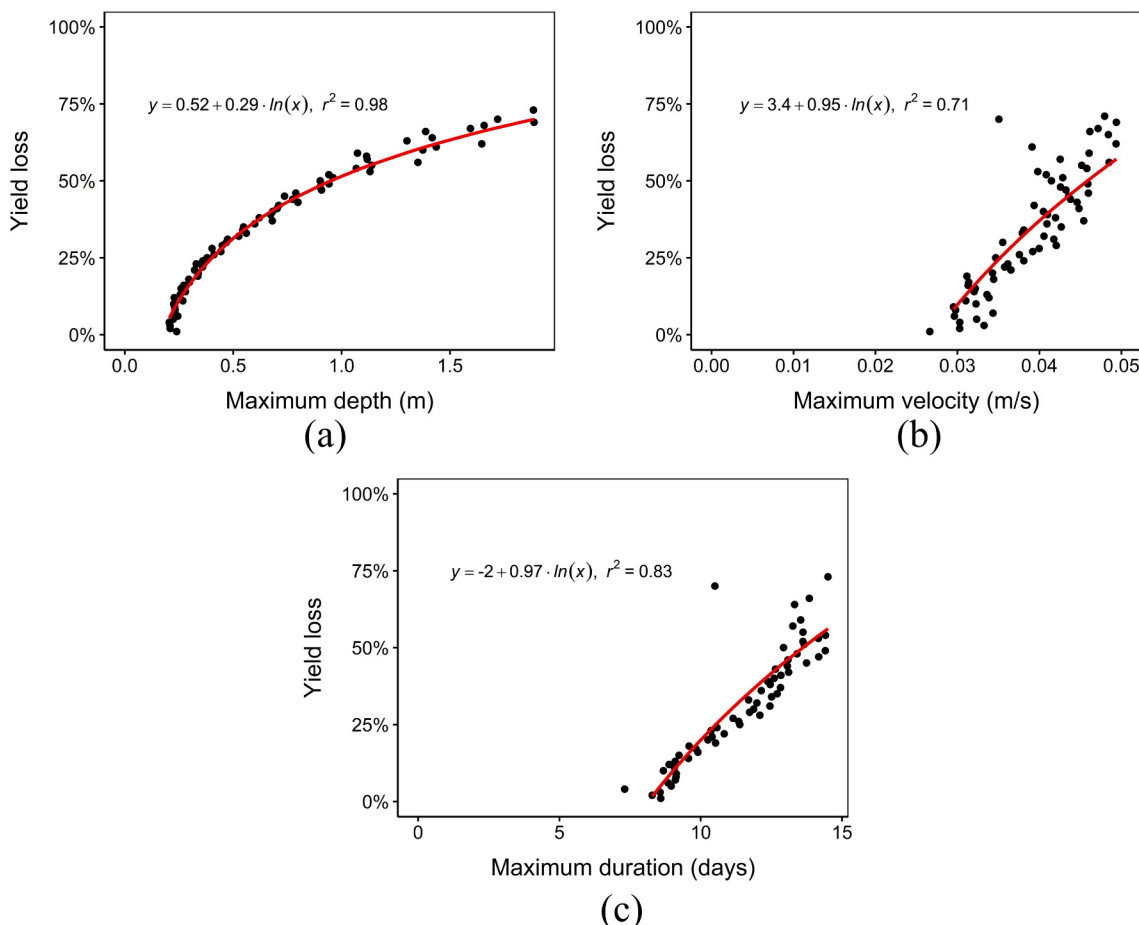


Fig. 13. Simulated vulnerability curve as a relationship between the intensity of flood parameters and the degree of yield loss. Red lines denote the fit logarithmic regression curve. (For interpretation of the references to colour in this figure legend, the reader is referred to the Web version of this article.)

Table 7

Regression function for proposed vulnerability curves; y is the rice crop yield loss (%) and x represents the maximum depth (m), velocity (m/s), and duration (days).

Flood parameter	Regression equations
Maximum depth (m)	$y = 0.52 + 0.29 \cdot \ln(x)$
Maximum velocity (m/s)	$y = 3.4 + 0.95 \cdot \ln(x)$
Maximum duration (days)	$y = -2 + 0.97 \cdot \ln(x)$

[23]; thus trend in a longer period of data (e.g., VHI, VCI) and inclusion of other climatology parameters (e.g., temperature for TCI) may not be suitable for this case study. Nevertheless, as pointed out by Yu et al.

[93], any VIs can be used to detect flood impacts on crops, even though most of them were originally developed for the case of drought impact [23].

Lastly, in the present study the relationship between the intensity of flood parameters and the degree of yield change relies on the statistical characteristic of the simulated output. Its characteristics, such as center, spread, and shape of the data distribution, determine its relationship. For instance, based on the simulation results, the value ranges of the crop yield change and the intensity of flood parameters obtained in this study are limited. Since the data range and distribution of the output values are subject to change for other case studies, this adds other changes to the vulnerability curve result. As mentioned in the previous study [51], such statistical relationships should be treated with care, as

Table 8

Comparison of damageable depth for minimum, half, and maximum yield loss flood from several previous studies.

No	Study	Condition	Damageable depth for respective yield loss (m)			Method
			Minimum loss (0%)	Half loss (50%)	Maximum loss (100%)	
1	Mekong [40]	13 days inundation	0.5	1	1.5	–
2	Philippines [31]	>7 days inundation in the maturity stage	0.5	0.8	1.2	Empirical data, expert and farmer's knowledge
3	Bangladesh [56]	16 days inundation	0.3	0.5	1	Observed data
4	Myanmar [32]	14 days inundation in the reproductive stage	0	2.3	3.4	Farmer interview and statistical model
5	Asia [86]	–	0	1.4	6	Literature study
6	This study	–	0.2	1	5.2	Remote sensing, flood modeling, and statistical model

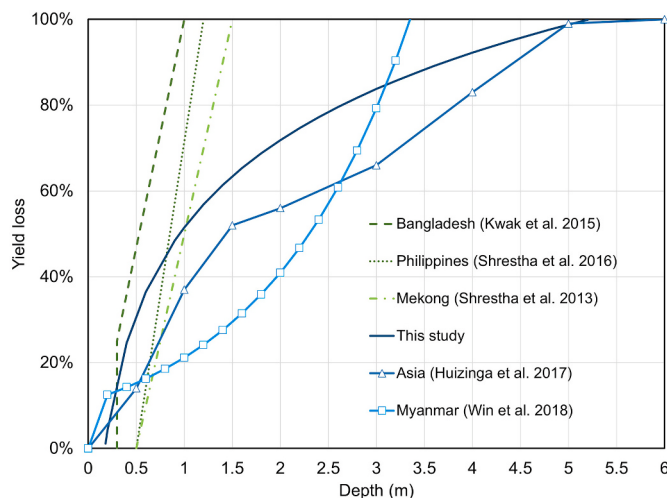


Fig. 14. Comparison of flood vulnerability curves for rice crop from several previous studies.

they do not represent the real physical relationship.

6. Conclusion

This study aimed to propose flood vulnerability curves or damage functions for rice crop using remote sensing and hydrodynamic modeling. Crop yield change and loss in grid-scale were obtained using multiple linear regression based on MODIS vegetation indices and city-scale crop yield statistics. The flood simulation of the Solo river basin's 2007 flood event was done using the RRI model. The degree of crop yield change and flood characteristics were compared, to derive the vulnerability curves.

In agreement with previous studies, our results reveal that water depth may be the most significant parameter to estimate the loss. In this study, the relationship between the intensity of flood parameters and the degree of yield loss fit logarithmic regression functions with R^2 of 0.98, 0.71, and 0.83 for depth, velocity, and duration relationship, respectively. Moreover, this study investigated the minimum and maximum damageable flood intensity at which rice crop is affected with minimum (0%) and maximum (100%) yield loss, respectively. For water depth, flow velocity, and duration relationship, the minimum damageable values are 0.2 m, 0.03 m/s, and 8 days, respectively, while the maximum damageable values (inducing complete yield loss) are 5.2 m, 0.08 m/s, and 22 days, respectively. Given depth as an important parameter, these results are generally in agreement with the previous studies that exhibited minimum and maximum damage depth ranging from 0 to 6 m.

This study provides an operational framework to derive flood vulnerability curves or flood damage functions for rice crops, especially for data-scarce regions. Some elaborations derived from experimentation and historical damage data are seen as pieces of important knowledge regarding the physical interaction between a crop plant and flood submergence. Moreover, experimental and empirical findings should be extended to real-world applications in large scale flood damage assessment (e.g., at river basin scale). As of now, the gaps between micro-plant scale understanding and macro-scale flood-crop loss assessment, as well as its applications among different regions, are still large. Since the use of a vulnerability curve is still preferable for flood assessment, finding a benchmark of flood intensity and crop yield loss relationship is required for future studies.

Declaration of competing interest

The authors declare that they have no known competing financial interests or personal relationships that could have appeared to influence

the work reported in this paper.

Acknowledgment

The acknowledgment was gratefully given to the Solo river basin organization (BBWSBS) for providing the observation data and Dr. Wonsik Kim for useful comments during discussion. We also thank anonymous reviewers for their constructive comments and suggestions, which led to substantial improvements of our manuscript.

Appendix A. Supplementary data

Supplementary data to this article can be found online at <https://doi.org/10.1016/j.ijdr.2021.102058>.

References

- [1] FAO, The Impact of Disasters on Agriculture and Food Security, vol. 77, FAO, Rome, 2015.
- [2] A. Singh, E.M. Septiningsih, H.S. Balyan, N.K. Singh, V. Rai, Genetics, physiological mechanisms and breeding of flood-tolerant rice (*oryza sativa* L.), *Plant Cell Physiol.* 58 (2) (2017) 185–197.
- [3] K. Kyuma, Nature and agriculture in monsoon Asia, *World* 13 (3) (2003).
- [4] H. Asada, J. Matsumoto, R. Rahman, Impact of recent severe floods on rice production in Bangladesh, *Geogr. Rev. Jpn.* 78 (12) (2005) 783–793.
- [5] M.M.Q. Mirza, Climate change, flooding in South Asia and implications, *Reg. Environ. Change* 11 (1) (2011) 95–107.
- [6] A.M. Ismail, U.S. Singh, S. Singh, M.H. Dar, D.J. Mackill, The contribution of submergence-tolerant (Sub1) rice varieties to food security in flood-prone rainfed lowland areas in Asia, *Field Crop. Res.* 152 (2013) 83–93.
- [7] D.J. Mackill, A.M. Ismail, U.S. Singh, R.V. Labios, T.R. Paris, Development and rapid adoption of submergence-tolerant (Sub1) rice varieties, *Adv. Agron.* 115 (2012) 303–356.
- [8] R.P. Rötter, M. Appiah, E. Fichtler, K.C. Kersebaum, M. Trnka, M.P. Hoffmann, Linking modelling and experimentation to better capture crop impacts of agroclimatic extremes—a review, *Field Crop. Res.* 221 (2018) 142–156.
- [9] D. Molinari, A.R. Scorzini, A. Gallazzi, F. Ballio, AGRIDE-c, a conceptual model for the estimation of flood damage to crops: development and implementation, *Nat. Hazards Earth Syst. Sci. Discuss.* (2019) 1–24.
- [10] B. Merz, H. Kreibich, R. Schwarze, A. Thielen, Review article "Assessment of economic flood damage, *Nat. Hazards Earth Syst. Sci.* 10 (8) (2010) 1697–1724.
- [11] S. Förster, B. Kuhlmann, K.E. Lindenschmidt, A. Bronstert, Assessing flood risk for a rural detention area, *Nat. Hazards Earth Syst. Sci.* 8 (2) (2008) 311–322.
- [12] S. Klaus, H. Kreibich, B. Merz, B. Kuhlmann, K. Schröter, Large-scale, seasonal flood risk analysis for agricultural crops in Germany, *Environ. Earth Sci.* 75 (18) (2016) 1289.
- [13] P.Q. Giang, T.T. Phuong, Evaluation of loss of rice production due to climate change reinforced flood in vietnam using hydrological model and GIS, *EnvironmentAsia* 11 (3) (2018).
- [14] H. Posthumus, J. Morris, T.M. Hess, D. Neville, E. Phillips, A. Baylis, Impacts of the summer 2007 floods on agriculture in England, *J. Flood Risk Manag.* 2 (3) (2009) 182–189.
- [15] E. Penning-Rowsell, C. Johnson, S. Tunstall, S. Tapsell, J. Morris, J. Chatterton, C. Green, The Benefits of Flood and Coastal Risk Management: a Handbook of Assessment Techniques, 2005, ISBN 1904750516.
- [16] D.I. Smith, Flood damage estimation—A review of urban stage-damage curves and loss functions, *WaterSA* 20 (3) (1994) 231–238.
- [17] T. Gerl, H. Kreibich, G. Franco, D. Marechal, K. Schröter, A review of flood loss models as basis for harmonization and benchmarking, *PloS One* 11 (7) (2016), e0159791, <https://doi.org/10.1371/journal.pone.0159791>.
- [18] Y. Budiyono, J. Aerts, J. Brinkman, M.A. Marfai, P. Ward, Flood risk assessment for delta mega-cities: a case study of Jakarta, *Nat. Hazards* 75 (1) (2015) 389–413.
- [19] M. Papathoma-Köhle, Vulnerability curves vs. vulnerability indicators: application of an indicator-based methodology for debris-flow hazards, *Nat. Hazards Earth Syst. Sci.* 16 (2016) 1771–1790, <https://doi.org/10.5194/nhess-16-1771-2016>.
- [20] J. Englhardt, H. de Moel, C.K. Huuyck, M.C. de Ruiter, J.C.J.H. Aerts, P.J. Ward, Enhancement of large-scale flood risk assessments using building-material-based vulnerability curves for an object-based approach in urban and rural areas, *Nat. Hazards Earth Syst. Sci.* 19 (2019) 1703–1722, <https://doi.org/10.5194/nhess-19-1703-2019>.
- [21] UNISDR, Sendai framework for disaster risk reduction 2015–2030. <https://www.unisdr.org/publication/sendai-framework-disaster-risk-reduction-2015-2030>, 2015. (Accessed 25 April 2020).
- [22] H. de Moel, J.C.J.H. Aerts, Effect of uncertainty in land use, damage models and inundation depth on flood damage estimates, *Nat. Hazards* 58 (1) (2011) 407–425.
- [23] M.S. Rahman, L. Di, A systematic review on case studies of remote-sensing-based flood crop loss assessment, *Agriculture* 10 (4) (2020) 131, <https://doi.org/10.3390/agriculture10040131>.
- [24] P. Brémond, F. Grelot, A.L. Agenais, Economic evaluation of flood damage to agriculture—review and analysis of existing methods, *Nat. Hazards Earth Syst. Sci.* 13 (10) (2013) 2493–2512.

- [25] Z. Ganji, A. Shokohi, J.M. Samani, Developing an agricultural flood loss estimation function (case study: rice), *Nat. Hazards* 64 (1) (2012) 405–419.
- [26] W. Buck, U. Merkel, Auswertung der HOWAS-Schadendatenbank, (Analysis of the HOWAS data base), Institut für Wasserwirtschaft und Kultertechnik der Universität Karlsruhe, 1999.
- [27] USACE, Flood Damage Analysis Package on the Microcomputer: User's Manual, Hydrologic Engineering Center, US Army Corps of Engineers, Davis, CA, 1988.
- [28] E. Penning-Rowell, S. Priest, D. Parker, J. Morris, S. Tunstall, C. Viavattene, J. Chatterton, D. Owen, *Flood and Coastal Erosion Risk Management: a Manual for Economic Appraisal*, Routledge, 2014.
- [29] D. Dutta, S. Herath, K. Musiakie, A mathematical model for flood loss estimation, *Journal Hydrol.* 277 (1–2) (2003) 24–49.
- [30] P. Brémont, F. Grelot, Comparison of a Systemic Modelling of Farm Vulnerability and Classical Methods to Appraise Flood Damage on Agricultural Activities, Advancing Sustainability in a Time of Crisis, 11th biennial conference of the International Society for Ecological Economics, August 22–25, Oldenburg and Bremen, Germany, 2010.
- [31] B.B. Shrestha, T. Okazumi, M. Miyamoto, H. Sawano, Flood damage assessment in the Pampanga river basin of the Philippines, *J. Flood Risk Manag.* 9 (4) (2016) 355–369.
- [32] S. Win, W.W. Zin, A. Kawasaki, Z.M.L.T. San, Establishment of flood damage function models: a case study in the Bago River Basin, Myanmar, *Int. J. Disaster Risk Reduct.* 28 (2018) 688–700.
- [33] A.E.K. Vozinaki, G.P. Karatzas, I.A. Sibetheros, E.A. Varouchakis, An agricultural flash flood loss estimation methodology: the case study of the Koiliaris basin (Greece), February 2003 flood, *Nat. Hazards* 79 (2) (2015) 899–920.
- [34] N.N. Kourgiolas, G.P. Karatzas, A hydro-economic modelling framework for flood damage estimation and the role of riparian vegetation, *Hydrol. Process.* 27 (4) (2013) 515–531.
- [35] J.M. Pivot, P. Martin, Farms adaptation to changes in flood risk: a management approach, *J. Hydrol.* 267 (1–2) (2002) 12–25.
- [36] Y. Hattori, K. Nagai, M. Ashikari, Rice growth adapting to deepwater, *Curr. Opin. Plant Biol.* 14 (1) (2011) 100–105.
- [37] S. Nishiuchi, T. Yamauchi, H. Takahashi, L. Kotula, M. Nakazono, Mechanisms for coping with submergence and waterlogging in rice, *Rice* 5 (1) (2012) 2.
- [38] S. Kazama, A. Sato, S. Kawagoe, Evaluating the cost of flood damage based on changes in extreme rainfall in Japan, *Sustain. Sci.* 4 (2009) 61.
- [39] S. Tezuka, H. Takiguchi, S. Kazama, A. Sato, S. Kawagoe, R. Sarukkalige, Estimation of the effects of climate change on flood-triggered economic losses in Japan, *Int. J. Disaster Risk Reduct.* 9 (2014) 58–67.
- [40] B.B. Shrestha, T. Okazumi, S. Tanaka, A. Sugiyura, Y. Kwak, S. Hibino, Development of flood vulnerability indices for lower Mekong basin in cambodain floodplain, *J. Jpn. Soc. Civil Eng. Ser. B1 (Hydraulic Eng.)* 69 (4) (2013) 1.1–1.6.
- [41] K. Takeuchi, A.W. Jayawardena, Y. Takahasi, Y. Tachikawa, Catalogue of Rivers for Southeast Asia and the Pacific, UNESCO-IHP Regional Steering Committee for Southeast Asia and the Pacific, Japan, 2004, p. 338.
- [42] BPS, Sensus Pertanian 2013 (Census of Agriculture 2013), 2013. <https://st2013.bps.go.id/>. (Accessed 7 June 2019).
- [43] World Bank, Agriculture, forestry, and fishing, value added (% of GDP). <http://data.worldbank.org/indicator/NV.AGR.TOTL.ZS>, 2017. (Accessed 8 June 2017).
- [44] BBWSBS, Profil Pengelolaan Sumber Daya Air Wilayah Sungai Bengawan Solo (Profile of Water Resources Management in Bengawan Solo River Basin), Ministry of Public Works and Public Housing, Solo, 2012.
- [45] H.G. Mawandha, B.S. Wigynosukarto, R. Jayadi, Mini polders as alternative flood management in the lower bengawan Solo river, Indonesia, *Irrigat. Drain.* 67 (2018) 72–80.
- [46] F. Hidayat, M.H. Harianto, *Impact of Climate Change on Floods in Bengawan Solo and Brantas River Basins*, 2008.
- [47] G.R. Brakenridge, Global Active Archive of Large Flood Events, Dartmouth Flood Observatory, University of Colorado. <http://floodobservatory.colorado.edu/Archives/index.html>, 2017. (Accessed 3 October 2017).
- [48] B.B. Shrestha, E.D.P. Perera, S. Kudo, M. Miyamoto, Y. Yamazaki, D. Kurabayashi, H. Sawano, T. Sayama, J. Magome, A. Hasegawa, T. Ushiyama, Assessing flood disaster impacts in agriculture under climate change in the river basins of Southeast Asia, *Nat. Hazards* 97 (1) (2019) 157–192.
- [49] N.A. Quarmy, M. Milnes, T.L. Hindle, N. Silleos, The use of multi-temporal NDVI measurements from AVHRR data for crop yield estimation and prediction, *Int. J. Rem. Sens.* 14 (2) (1993) 199–210.
- [50] E. Pantaleoni, B.A. Engel, C.J. Johannsen, Identifying agricultural flood damage using Landsat imagery, *Precis. Agric.* 8 (1–2) (2007) 27–36.
- [51] H. Chen, Z. Liang, Y. Liu, Q. Liang, S. Xie, Integrated remote sensing imagery and two-dimensional hydraulic modeling approach for impact evaluation of flood on crop yields, *J. Hydrol.* 553 (2017) 262–275.
- [52] C. Funk, M.E. Budde, Phenologically-tuned MODIS NDVI-based production anomaly estimates for Zimbabwe, *Rem.Sens. Environ.* 113 (1) (2009) 115–125.
- [53] M.S. Mkhabela, P. Bullock, S. Raj, S. Wang, Y. Yang, Crop yield forecasting on the Canadian Prairies using MODIS NDVI data, *Agric. For. Meteorol.* 151 (3) (2011) 385–393.
- [54] N.T. Son, C.F. Chen, C.R. Chen, V.Q. Minh, N.H. Trung, A comparative analysis of multitemporal MODIS EVI and NDVI data for large-scale rice yield estimation, *Agric. For. Meteorol.* 197 (2014) 52–64.
- [55] M.F. Lopresti, C.M. Di Bella, A.J. Degioanni, Relationship between MODIS-NDVI data and wheat yield: a case study in Northern Buenos Aires province, Argentina, *Inform. Process. Agric.* 2 (2) (2015) 73–84.
- [56] Y. Kwak, B. Arifuzzaman, Y. Iwami, Prompt proxy mapping of flood damaged rice fields using MODIS-derived indices, *Rem. Sens.* 7 (12) (2015) 15969–15988.
- [57] R. Shrestha, L. Di, G.Y. Eugene, L. Kang, Y.Z. Shao, Y.Q. Bai, Regression model to estimate flood impact on corn yield using MODIS NDVI and USDA cropland data layer, *J. Integrat. Agric.* 16 (2) (2017) 398–407.
- [58] T. Sayama, G. Ozawa, T. Kawakami, S. Nabesaka, K. Fukami, Rainfall-Runoff-Inundation analysis of Pakistan flood 2010 at the Kabul river basin, *Hydrol. Sci. J.* 57 (2) (2012), <https://doi.org/10.1080/02626667.2011.644245>.
- [59] A. Huete, K. Didan, T. Miura, E.P. Rodriguez, X. Gao, L.G. Ferreira, Overview of the radiometric and biophysical performance of the MODIS vegetation indices, *Rem. Sens. Environ.* 83 (1–2) (2002) 195–213.
- [60] N. Guindin-Garcia, A.A. Gitelson, T.J. Arkebauer, J. Shanahan, A. Weiss, An evaluation of MODIS 8-and 16-day composite products for monitoring maize green leaf area index, *Agric. For. Meteorol.* 161 (2012) 15–25.
- [61] S. Testa, E.C.B. Mondino, C. Pedrola, Correcting MODIS 16-day composite NDVI time-series with actual acquisition dates, *Eur. J. Rem. Sens.* 47 (1) (2014) 285–305.
- [62] T. Sayama, Rainfall-runoff-inundation (RRI) model technical manual, Technical Note of PWRI (2014) 4277.
- [63] S.S. Bhagabati, A. Kawasaki, Consideration of the rainfall-runoff-inundation (RRI) model for flood mapping in a deltaic area of Myanmar, *Hydrol. Res. Lett.* 11 (3) (2017) 155–160.
- [64] Z.M. Khaing, K. Zhang, H. Sawano, B.B. Shrestha, T. Sayama, K. Nakamura, Flood hazard mapping and assessment in data-scarce Nyaungdon area, Myanmar, *PLoS One* 14 (11) (2019), e0224558.
- [65] B. Lehner, K. Verdin, A. Jarvis, New global hydrography derived from spaceborne elevation data, *Eos, Trans. Am. Geophys. Union* 89 (10) (2008) 93–94.
- [66] W. Zhu, Y. Pan, H. He, L. Wang, M. Mou, J. Liu, A changing weight filter method for reconstructing a high-quality NDVI time series to preserve the integrity of vegetation phenology, *IEEE Trans. Geosci. Rem. Sens.* 50 (2012) 1085–1095, <https://doi.org/10.1109/TGRS.2011.2166965>.
- [67] M.R. Ahmed, K.R. Rahaman, A. Kok, Q.K. Hassan, Remote sensing-based quantification of the impact of flash flooding on the rice production: a case study over Northeastern Bangladesh, *Sensors* 17 (10) (2017) 2347, <https://doi.org/10.3390/s17102347>.
- [68] J. Ren, Z. Chen, Q. Zhou, H. Tang, Regional yield estimation for winter wheat with MODIS-NDVI data in Shandong, China, *Int. J. Appl. Earth Obs. Geoinf.* 10 (4) (2008) 403–413.
- [69] J.N. Hird, G.J. McDermid, Noise reduction of NDVI time series: an empirical comparison of selected techniques, *Rem.Sens. Environ.* 113 (1) (2009) 248–258.
- [70] L. Eklundh, P. Jönsson, TIMESAT: A Software Package for Time-Series Processing and Assessment of Vegetation Dynamics. *Remote Sensing Time Series*, Springer, Cham, 2015, pp. 141–158.
- [71] R. Balaghi, B. Tychon, H. Eerens, M. Jlibene, Empirical regression models using NDVI, rainfall and temperature data for the early prediction of wheat grain yields in Morocco, *Int. J. Appl. Earth Obs. Geoinf.* 10 (4) (2008) 438–452.
- [72] J. Huang, X. Wang, X. Li, H. Tian, Z. Pan, Remotely sensed rice yield prediction using multi-temporal NDVI data derived from NOAA's-AVHRR, *PLoS One* 8 (8) (2013), e70816.
- [73] S. Kudo, T. Sayama, A. Hasegawa, A. Iwami, June. Analysis of flood risk change in future climate in terms of discharge and inundation in the Solo River Basin, in: *Proceedings of the 7th International Conference on Water Resources and Environment Research—ICWRER*, 2016.
- [74] S. Yoshimoto, G. Amarnath, Applications of satellite-based rainfall estimates in flood inundation modeling—a case study in Mundeni Aru River Basin, Sri Lanka, *Rem. Sens.* 9 (10) (2017) 998.
- [75] J. Han, J. Pei, M. Kamber, *Data Mining: Concepts and Techniques*, Elsevier, 2011.
- [76] J.E. Nash, J.V. Sutcliffe, River flow forecasting through conceptual models part I—a discussion of principles, *Journal Hydrol.* 10 (3) (1970) 282–290.
- [77] P.D. Bates, A.P.J. De Roo, A simple raster-based model for flood inundation simulation, *Journal Hydrol.* 236 (1–2) (2000) 54–77.
- [78] D.N. Moriasi, J.G. Arnold, M.W. Van Liew, R.L. Bingner, R.D. Harmel, T.L. Veith, Model evaluation guidelines for systematic quantification of accuracy in watershed simulations, *Trans. ASABE* 50 (3) (2007) 885–900.
- [79] V. Te Chow, *Applied Hydrology*, Tata McGraw-Hill Education, 2010.
- [80] M.K. Rowshon, M.S.M. Amin, M.A. Mojid, M. Yaji, Estimated evapotranspiration of rice based on pan evaporation as a surrogate to lysimeter measurement, *Paddy Water Environ.* 12 (1) (2014) 35–41.
- [81] N.V. Nguyen, *Global Climate Changes and Rice Food Security*, FAO, Rome, 2002.
- [82] A. Kotera, E. Nawata, L.V. Thao, N. Van Vuong, T. Sakuratani, Effect of submergence on rice yield in the red river delta, vietnam, *Jpn. J. Trop. Agric.* 49 (3) (2005) 197–206.
- [83] E.M. Septiningisih, A.M. Pamplona, D.L. Sanchez, C.N. Neeraja, G.V. Vergara, S. Heuer, A.M. Ismail, D.J. Mackill, Development of submergence-tolerant rice cultivars: the Sub1 locus and beyond, *Ann. Bot.* 103 (2) (2009) 151–160.
- [84] M.H. Dar, A. De Janvry, K. Emerick, D. Raitzer, E. Sadoulet, Flood-tolerant rice reduces yield variability and raises expected yield, differentially benefiting socially disadvantaged groups, *Sci. Rep.* 3 (2013) 3315.
- [85] Y. Zhang, Z. Wang, L. Li, Q. Zhou, Y. Xiao, X. Wei, M. Zhou, Short-term complete submergence of rice at the tillering stage increases yield, *PLoS One* 10 (5) (2015), e0127982.
- [86] J. Huizinga, H. De Moel, W. Szewczyk, *Global Flood Depth-Damage Functions: Methodology and the Database with Guidelines (No. JRC105688)*, Joint Research Centre, 2017.
- [87] A.R. Huete, A soil-adjusted vegetation index (SAVI), *Remote Sens. Environ.* 25 (1988) 295–309.

- [88] C.J. Tucker, Red and photographic infrared linear combinations for monitoring vegetation, *Rem. Sens. Environ.* 8 (2) (1979) 127–150.
- [89] F.N. Kogan, Remote sensing of weather impacts on vegetation in non-homogeneous areas, *Int. J. Rem. Sens.* 11 (8) (1990) 1405–1419.
- [90] F.N. Kogan, Droughts of the late 1980s in the United States as derived from NOAA polar-orbiting satellite data, *Bull. Am. Meteorol. Soc.* 76 (5) (1995) 655–668.
- [91] L. Di, E. Yu, R. Shrestha, L. Lin, July. DVDI: a new remotely sensed index for measuring vegetation damage caused by natural disasters, in: IGARSS 2018-2018 IEEE International Geoscience and Remote Sensing Symposium, IEEE, 2018, pp. 9067–9069, <https://doi.org/10.1109/IGARSS.2018.8518022>.
- [92] V.A. Bento, C.M. Gouveia, C.C. DaCamara, I.F. Trigo, A climatological assessment of drought impact on vegetation health index, *Agric. For. Meteorol.* 259 (2018) 286–295.
- [93] G. Yu, L. Di, B. Zhang, Y. Shao, R. Shrestha, L. Kang, Remote-sensing-based flood damage estimation using crop condition profiles, in: 2013 Second International Conference on Agro-Geoinformatics (Agro-Geoinformatics), IEEE, 2013, pp. 205–210, <https://doi.org/10.1109/Argo-Geoinformatics.2013.6621908>.